

# Space Weather

## RESEARCH ARTICLE

10.1029/2021SW002775

### Key Points:

- Uncertainties in the arrival time of interplanetary coronal mass ejection (ICMEs) derive from a mixture of individual, but identifiable uncertainties in the chain from the Sun to 1 AU
- Different ADAPT realizations produce uncertainties in the arrival time of ICMEs of  $\pm 7$  h or more
- Targeted studies aimed at reducing each of the uncertainties would improve the accuracy and precision in the arrival time of ICMEs

### Correspondence to:

P. Riley,  
[pete@predsci.com](mailto:pete@predsci.com)

### Citation:

Riley, P., & Ben-Nun, M. (2021). On the sources and sizes of uncertainty in predicting the arrival time of interplanetary coronal mass ejections using global MHD models. *Space Weather*, 19, e2021SW002775. <https://doi.org/10.1029/2021SW002775>

Received 31 MAR 2021

Accepted 28 MAY 2021

© 2021. The Authors.

This is an open access article under the terms of the [Creative Commons Attribution-NonCommercial License](#), which permits use, distribution and reproduction in any medium, provided the original work is properly cited and is not used for commercial purposes.

## On the Sources and Sizes of Uncertainty in Predicting the Arrival Time of Interplanetary Coronal Mass Ejections Using Global MHD Models

Pete Riley<sup>1</sup>  and Michal Ben-Nun<sup>1</sup> 

<sup>1</sup>Predictive Science Inc., San Diego, CA, USA

**Abstract** Accurate predictions of the properties of interplanetary coronal mass ejection (ICME)-driven disturbances are a key objective for space weather forecasts. The ICME's time of arrival (ToA) at Earth is an important parameter, and one that is amenable to a variety of modeling approaches. Previous studies suggest that the best models can predict the arrival time to within an absolute uncertainty of 10–15 h. Here, we investigate the main sources of uncertainty in predicting a CME's ToA at Earth. These can be broken into two main categories: (a) the initial properties of the ejecta, including its speed, mass, and direction of propagation and (b) the properties of the ambient solar wind into which it propagates. To estimate the relative contribution to ToA uncertainties, we construct a set of numerical experiments of cone-model CMEs, where we vary the initial speed, mass, and direction at the inner radial boundary. Additionally, we build an ensemble of 12 ambient solar wind solutions using realizations from the ADAPT model. We find that each component in the chain contributes between  $\pm 2.5$  and  $\pm 7$  h of uncertainty to the estimate of the CME's ToA. Importantly, different realizations of the synoptic produce the largest uncertainties. This suggests that estimates of ToA will continue to be plagued with intrinsic uncertainties of  $\pm 10$  h until tighter constraints can be found for these boundary conditions. Our results suggest that there are clear benefits to focused investigations aimed at reducing the uncertainties in CME speed, mass, direction, and input boundary magnetic fields.

**Plain Language Summary** Coronal mass ejections are huge explosions of plasma and magnetic field, which, if they impact the Earth's protective magnetospheric shield, can result in a range of consequences, from increased radiation doses for aircraft passengers to electrical blackouts across large regions. Being able to forecast their properties, as well as when they will arrive at Earth are key objectives for space weather programs. In this study, we have investigated a broad set of uncertainties associated with these predictions, which include the initial specification of the properties of the CME at the Sun as well as the properties of the interplanetary medium into which it propagates. Remarkably, and disappointingly, we find that there are inherent limitations in the accuracy of the forecasts that will not likely be resolved by more sophisticated modeling techniques. Instead, they will require substantial investment in developing more comprehensive datasets to drive the models, which, in turn, will require new space missions. More modest improvements, however, can be made by addressing components in the forecasting system and attempting to reduce (or at least accurately assess) the uncertainties associated with them.

## 1. Introduction

Geomagnetic storms are an essential component of space weather at Earth, and anticipating their onset is one of the major priorities for the National Oceanic and Atmospheric Administration (NOAA) Space Weather Prediction Center (SWPC). The two primary drivers of these storms are fast solar wind streams and coronal mass ejections (CMEs). CMEs are large-scale coronal eruptions that propel plasma and magnetic fields into the solar wind, and are generally responsible for the most severe storms (Gosling et al., 1990). To provide 1–4-day warning of these storms, NOAA/SWPC operationally implemented the Wang-Sheeley-Arge-ENLIL cone model, or WSA + ENLIL (Pizzo et al., 2011).

Ideally, a comprehensive CME forecasting framework would begin at the Sun, using first-principles models (e.g., Forbes & Lin, 2000), and provide the longest lead-time for predictions. However, in practice, models

capable of mimicking the eruption of the CME and its evolution in the corona remain idealized and the subject of fundamental research, not operational forecasting (Török et al., 2018). Thus, current forecasting models blend elements of empiricism and domain reduction to provide tractable solutions. For example, CMEs are often treated as hydrodynamic “pulses,” usually inserted high in the corona, with properties inferred from relevant observations (e.g., Odstrčil et al., 2004; Riley et al., 2003).

The WSA + ENLIL forecasting system is a good example of the general approach applied by a number of groups (Riley et al., 2018), and proceeds in the following manner: Magnetic maps of the solar magnetic field in the photosphere, obtained from ground- and/or space-based observatories (Riley et al., 2014), are used to compute potential field models of the solar corona. An empirical prescription for the solar wind speed based on magnetic field structure, the Wang-Sheeley-Argge (WSA) model (Arge et al., 2003), is used to specify boundary conditions for the ENLIL magnetohydrodynamic (MHD) model of the solar wind (Odstrčil et al., 2003). ENLIL is integrated in time until a steady-state background solar wind solution is reached beyond 1 AU. This solution is typically updated several times a day, as new magnetograms are made available. When observed, “cone-model” CMEs are injected into the flow and tracked out to 1 AU (e.g., Pizzo et al., 2011). Similar space weather systems have also been developed by other teams, such as the “European heliospheric forecasting information asset” (EUHFORIA) (Pomoell & Poedts, 2018) and the “Space-weather-forecast-Usable System Anchored by Numerical Operations and Observations – CME” (SUSANOO-CME) (Shiota & Kataoka, 2016). Other approaches, such as using interplanetary scintillation (IPS) to derive ambient solar wind conditions (e.g., Jackson et al., 2015) or track CME front (e.g., Iwai et al., 2019), while promising, have not yet been adopted within the operational environment.

Several previous studies have investigated the WSA + ENLIL forecasting system. Pizzo et al. (2015), for example, explored the effects of launching a range of cone-model CMEs into different idealized ambient solar wind states. In particular, they developed a set of idealized numerical experiments, propagating a series of CME pulses into (a) a uniform (spherically symmetric background) and (b) a tilted-dipole stream structure. They found relatively predictable patterns in the time of arrival (ToA) of ICMEs as a function of the initial properties of the ejecta, and ruled out the possibility of any chaotic behavior that might manifest itself in the forecasts.

Mays et al. (2015) developed ensemble model results for 35 observed CME events occurring between January 2013 and July 2014. For those events that were predicted to arrive at earth (17 events), they estimated the mean absolute error (MAE) in ToA prediction of 12.3 h. They also estimated correct and false-alarm ratios for these events. They suggested that the accuracy of the predicted arrival time was sensitive to the initial distribution of CME parameters, and that for their analyses, the spread was probably underestimated.

Riley et al. (2018) summarized a large number of CME forecasting tools and compared their forecasting capabilities with one another. They addressed: (a) How well the models predicted the arrival time of CME-driven shocks at Earth? (b) What were the errors associated with these forecasts? (c) Which, if any models performed better? and (d) Did any of the models had demonstrate improvements in accuracy over the 6-year period that they had been in use? They found that, for the best models, CME-shock arrival times could be predicted with  $\pm 1$  h (mean error) or  $\pm 13$  h (mean absolute error), with a precision (standard deviation) of 15 h. It is worth noting that while mean error is often used as a measure of accuracy, because positive and negative errors tend to cancel one another out, a more meaningful metric is MAE. On the other hand, the mean error remains important since it conveys information about any possible forecast bias, that is, the tendency for the model to systematically underestimate or overestimate the observed arrival time. Thus, in practice, it is often useful to track both parameters. Finally, Riley et al. (2018) also inferred that there had been no measurable improvement in model accuracy during the 6-year interval that predictions had been made.

More generally, a number of studies have explored various aspects of ensemble modeling of ICMEs (e.g., Amerstorfer et al., 2021; Dumbović et al., 2018; Kay et al., 2020). Kay et al. (2020), in particular, considering the sensitivity of ToA to various uncertainties in the model inputs, finding that for moderate ICMEs, speed was the most important parameter to estimate accurately. However, for more extreme events, the angular width of the ejecta was a more critical factor. Finally, Verbeke et al. (2019) described a community-driven benchmarking effort to adopt specific metrics, skill-scores, events and datasets to improve ICME predictions.

In this study, we build upon these earlier investigations in several important ways. First, we consider the propagation of CME pulses through a set of 12 ADAPT-GONG realizations of the photospheric magnetic field. These are estimates of the synchronic field that are, in principle all likely to be equally valid, or at least consistent with the available observations. Second, we consider the propagation of a large number of CME pulses that are representative of a fast CME with a distribution in properties that are consistent with the likely uncertainties in their measured values. Third, we estimate the contributions to the estimated uncertainties in arrival time due to each component (or model parameter) in the modeled system. We note in passing that “uncertainty” and “error” are often used interchangeably when describing the distribution in ToAs. Here, since we are characterizing the spread in values, and not attempting to match with a “correct” answer, we use the term “uncertainty” exclusively.

## 2. Methods

### 2.1. Data

For this study, we use ADAPT-GONG quasi-synchronic magnetograms (Arge et al., 2010). These are “quasi-” or “pseudo-” synchronic in the sense that only observations from Earth-based solar observatories are used to generate each map at each point in time, and photospheric magnetic flux transport processes are invoked to evolve the magnetic field distribution as it drifts westward and beyond the observation window. Additionally, data assimilation techniques are used to update the modeled flux with new observations. In principle, this can account for both model and observational uncertainties, and, importantly, allows for the generation of multiple realizations at each point in time. To compute MHD solutions, we further process the magnetograms by smoothing them, extrapolating mid-latitude data poleward, and removing any monopole components (e.g., Riley et al., 2012).

We chose Carrington Rotation (CR) 2207 (September 2, 2018–September 29, 2018) for our analysis since it occurred during a time period that was: (a) relatively stable from one rotation to the next, (b) exhibited a simple solar minimum-like configuration with slow flow emanating from about the equator and large polar coronal holes producing fast, steady solar wind at higher latitudes, and (c) devoid of any significant CME activity. Figure 1 summarizes 12 realizations of ADAPT/GONG synchronic maps corresponding to the mid-point in time of CR 2207.

We note several points. First, overall, the realizations look very similar to one another. The two main clusters of active regions (at 80° and 240°) appear to be nearly identical, as does the overall structure of the polar regions. It is worth noting, however, that the fields have been visually saturated at  $\pm 10$  G. Second, at smaller scales there are some subtle differences. For example, the structure of the polar regions, as evidenced by contours near  $\pm 10$  G (the boundary between deep red/blue and white), changes from one realization to the next. In particular, the white excursions into the otherwise red/blue polar regions occur at slightly different longitudes from one panel to the next. Third, the shape of the active region (AR) fields, including the orientation of the bipoles, changes modestly from one realization to the next. Additionally, the strength of the AR fields is not the same. For example, consider the negative flux region south of, but between the two major ARs at  $\sim 240^\circ$  longitude. This is much weaker in realization 11 than in realization 12. These are, however, minor differences, and it is not clear based only on these maps what impact, if any, they may have on the evolution of CMEs in the solar wind. Only by simulating an ICME through all solutions can we assess their impact on the ToA of the ICME. It is, however, worth underscoring that these ADAPT realizations are just that: synchronic maps that are all consistent with the available observations. Thus, we cannot – a priori – say that one is better than another, and so they provide a useful way to capture (or, at least, provide a lower limit to) uncertainties due to the ambient boundary conditions.

### 2.2. Models

#### 2.2.1. Ambient Solar Wind

Our goal in this study is not to attempt to find the best match between models of ICMEs and their observed signatures, but, for a range of typical values, to assess how sensitive the ToA of the event at Earth is to the various input parameters used to launch the CME. For this reason, it is not necessary to run the

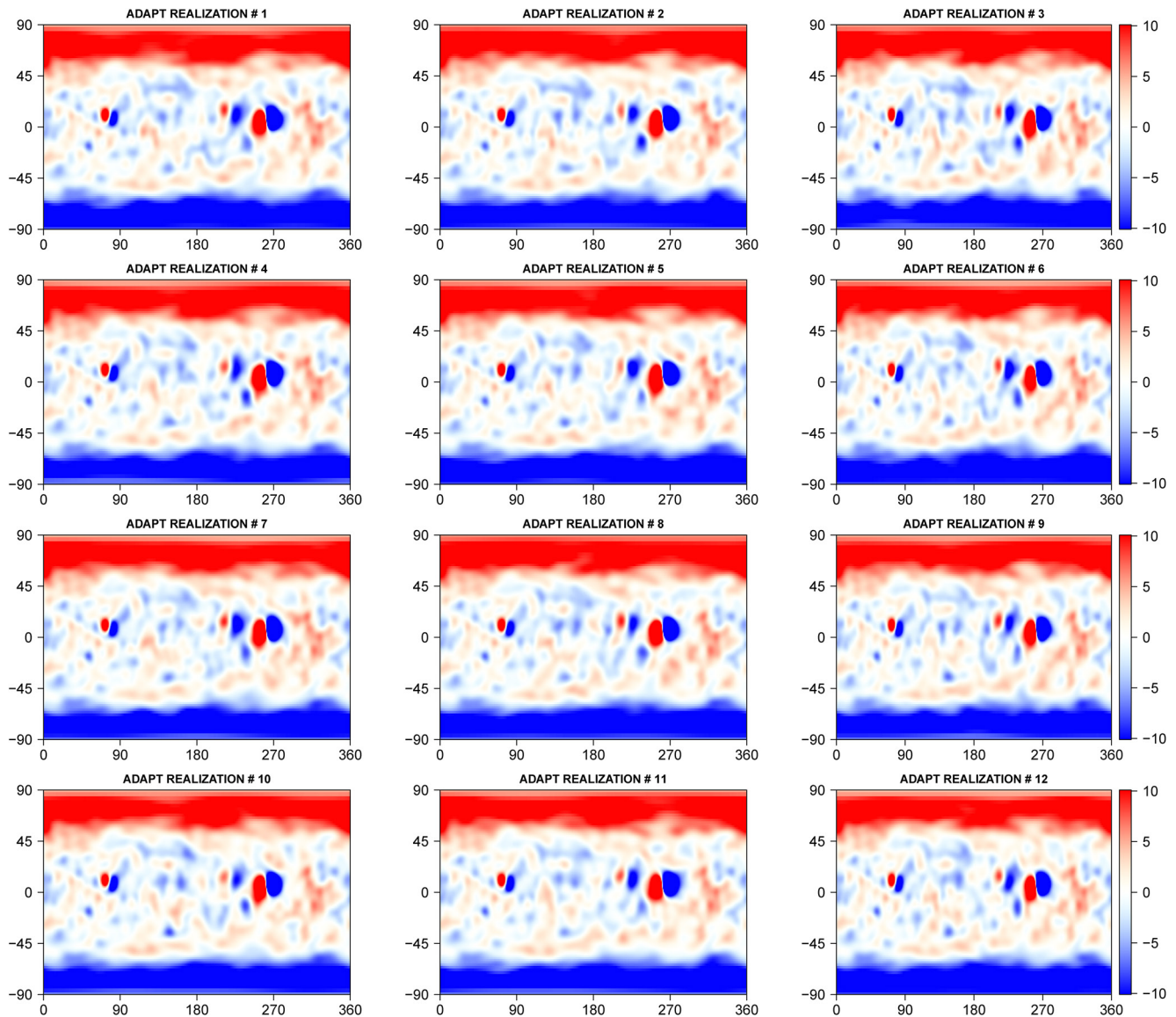


**Figure 1.** Twelve ADAPT Quasi-synchronic maps for Carrington rotation 2207. The panels have been saturated at  $\pm 10$  G.

most sophisticated numerical model. In fact, since the goal is to generate a large number of solutions to estimate uncertainties, we chose an empirical background model to generate the ambient solar wind Riley et al. (2001, 2012). In this approach, the magnetic field of the corona is computed using the observed photospheric field maps shown in Figure 1, and the structure of the field is used to generate the boundary conditions for the heliospheric simulation. In particular, we use the “Distance from the Coronal Hole” (DCHB) technique (Riley et al., 2001) to generate longitude-latitude maps of solar wind speed at the inner boundary of the heliospheric calculation (at  $30R_S$ ). The Radial component of the magnetic field is used directly from the coronal solution, and the other (normal) components of the field and velocity are set to zero. Pressure balance and momentum flux balance across the sphere at  $30R_S$  are used to specify the remaining magnetofluid parameters, temperature and density, respectively. This approach is similar in concept to that employed by WSA + ENLIL (Pizzo et al., 2015), except that WSA + ENLIL use expansion factor to specify the values of solar wind speed at the inner radial boundary of the heliospheric model. Although we have demonstrated that the DCHB method is generally more accurate than the WSA approach (Riley et al., 2015), for the purposes of this investigation, either approach could be justified. More importantly, the results presented here, and the inferences drawn from them, would not differ substantially.



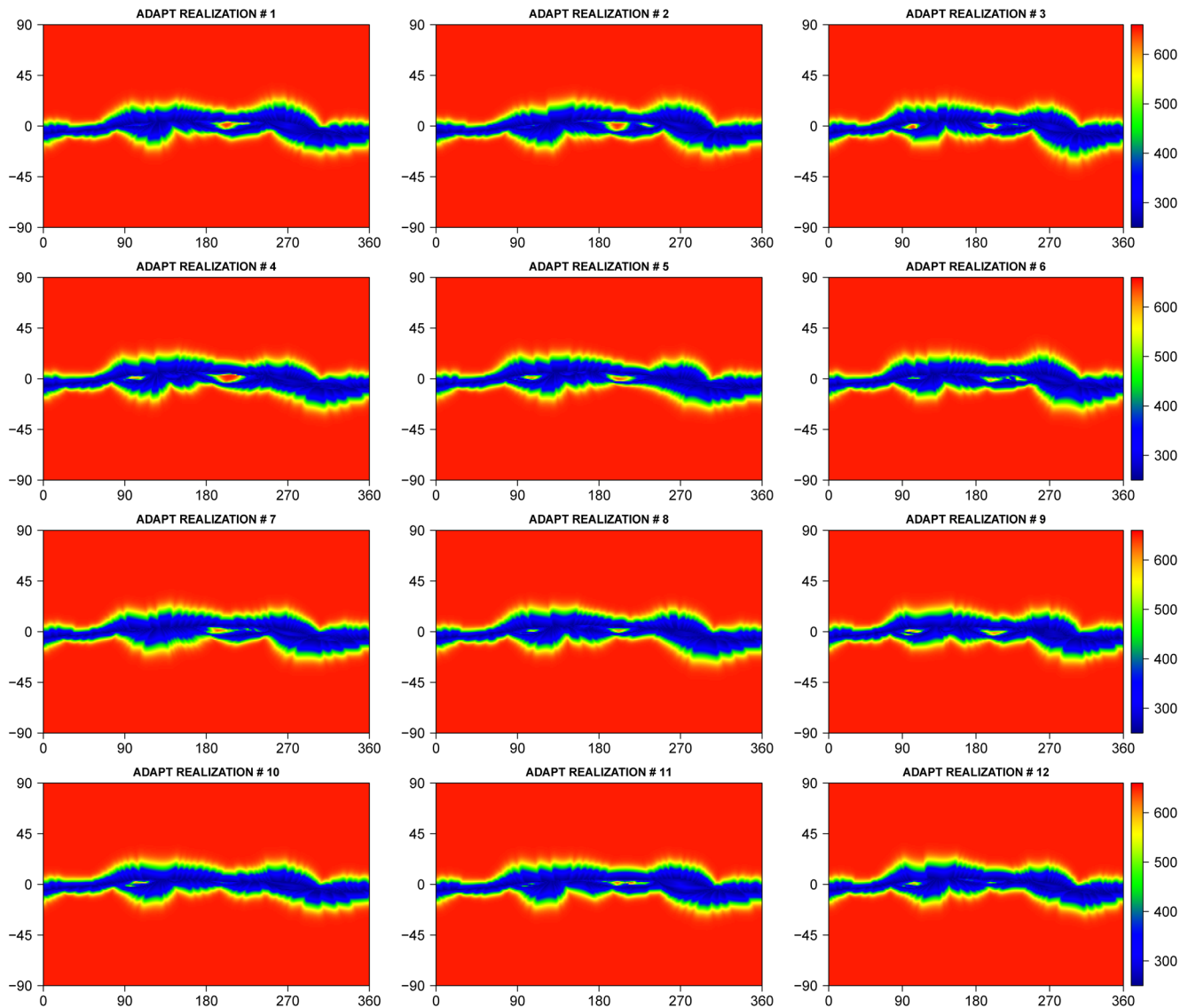


**Figure 2.** Computed radial speed at the inner boundary of the heliospheric model for Carrington rotation 2207.

Figure 2 shows the computed radial speed at the inner boundary of the heliospheric calculation for the synchronic maps shown in Figure 1. We can make the same general comments about the overall similarity between each of the panels, but again, note the appearance of more subtle smaller-scale differences. In fact, these differences are more noticeable in the boundary conditions for solar wind speed than they were for the photospheric magnetic field, with the longitudinal alignment of fast-slow (or slow-fast) boundaries shifting by  $5^{\circ}$ – $10^{\circ}$  in some cases. Additionally, the relative orientation (in the latitude-longitude plane) of the fast-slow boundaries changes from one realization to the next. Although it is possible to infer how these differences will evolve (at least qualitatively) as the plasma propagates away from the Sun, it is difficult, if not impossible to reliably deduce how CME propagation (and deformation) will be affected by the differences.

Finally, in Figure 3 we explore the variations amongst the 12 ADAPT realizations for CR 2207 in terms of (a) the magnetic field maps and (b) the radial speeds used to drive the heliospheric model. Focusing first on the magnetic field map variations, we note several points. First, where current Earth-based observations are directly contributing to the maps (in the longitudinal range from  $-60^{\circ}$  ( $300^{\circ}$ ) to  $+60^{\circ}$ ), there are no significant differences. Additionally, the eastern edge of this region is sharp, whereas the western boundary merges smoothly into the far-side of the Sun, reflecting the process by which the images are assimilated.

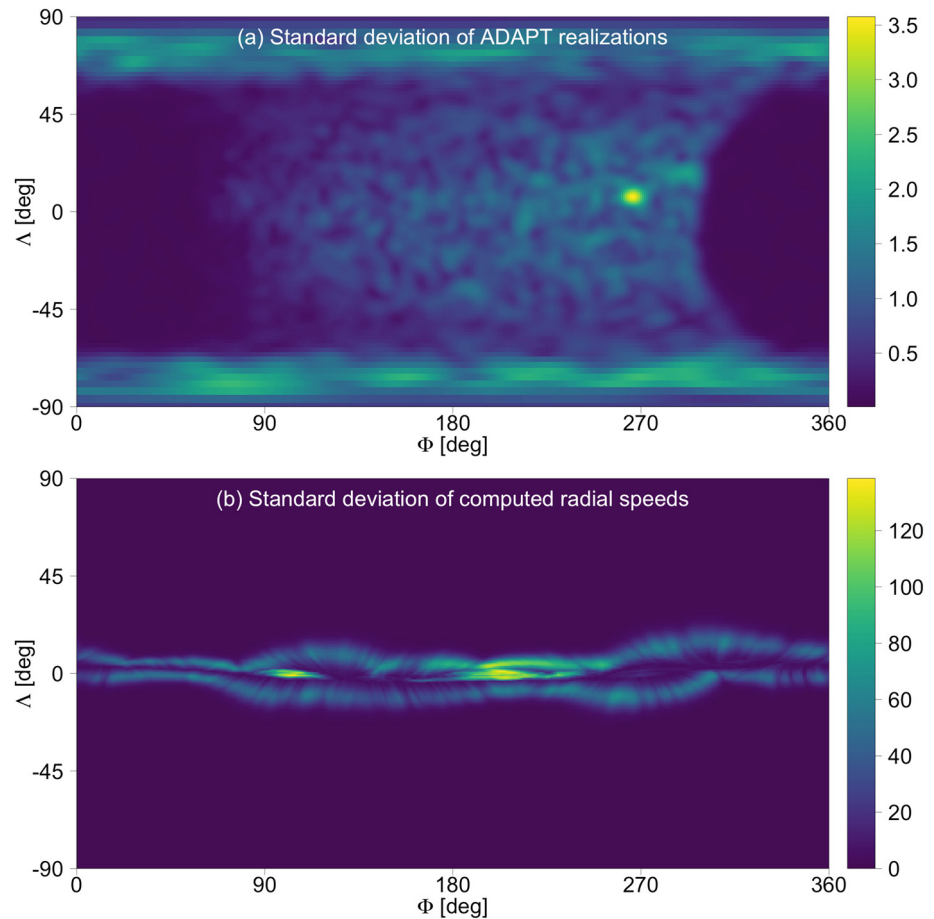


**Figure 3.** The standard deviations of (a) the ADAPT map realizations from Figure 1 and (b) the computed radial speed at the inner boundary of the heliospheric model from Figure 2, both for Carrington rotation 2207.

Second the differences are largest at the polar regions, showing a characteristic scale size of  $60^{\circ}$ – $90^{\circ}$ . Third, the single, largest variability is associated with the AR centered at  $\sim 270^{\circ}$  longitude, just above the heliographic equator.

In contrast to the variability amongst the ADAPT maps, the standard deviation of the computed radial speeds is largest in a narrow band around the heliographic equator. Comparison with Figure 2 reveals that the two “fuzzy” bands are centered on the transition from slow to fast wind in each hemisphere, while the largest variability at  $\sim 200^{\circ}$  longitude captures the differences in the location and size of the equatorial coronal hole near there. Similarly, the large variability at  $\sim 90^{\circ}$  longitude is due to the a second, smaller coronal hole. Finally, it is worth noting that the variations in the photospheric magnetic fields and computed radial speeds are related. The structure of the polar magnetic field variations maps into the “fuzzy” bands in speed, while albeit more indirectly, the differences in the location and size of the ARs, and particularly the one at  $\sim 270^{\circ}$  longitude are responsible for the offsets and sizes of the two equatorial coronal holes.

### 2.2.2. CME Pulses

To mimic the launch of a CME from the upper corona, we follow the same prescription as other forecasting teams, by specifying the location, direction, speed, temperature, and density (or mass) of the ejecta as it passes through the inner radial boundary of the simulation. For the purposes of brevity, we report here on the following permutations: (1) Speed – 800, 1,000, and 1,200  $\text{km s}^{-1}$ ; (2) Density –  $\times 1$ ,  $\times 2$ , and  $\times 4$  enhancement over a background base density of  $500 \text{ cm}^{-3}$ ; and (3) Propagation direction/location – 100 radial traces within a  $15^{\circ}$  circle about the CME’s launch center. The temperature was assumed to be that of the ambient slow solar wind and the direction of propagation was assumed to be radial. Taken together, these

variations represent reasonable uncertainties in the initial properties of CMEs observed in white light. The CME pulse is launched through the inner radial boundary by smoothly raising the variable's value over a one-hour interval, keeping it constant for the next 12 h, and then smoothly returning it to ambient values over a one-hour interval. In the transverse plane, the CME is given a circular profile with a total angular width of  $30^\circ$ . Although the precise shape of the CME's profile can have a modest impact on the resulting structure of the ICME farther out in the solar wind (e.g., Riley & Gosling, 1998), it does not impact the analysis presented here.

With three inputs each for speed and density, 100 values for “location,” and, for all of these combinations, 12 realizations of the ambient solar wind, there are a total of 10,800 plausible time series that could be observed at Earth. Again, we reiterate that, as a sensitivity study, there is no “ground truth” answer concerning which is the most correct, only different clusters of results to estimate the relative contribution to uncertainties due to our incomplete knowledge of the properties of the CME or the ambient solar wind into which it is propagating.

Regarding the “location” variable, rather than simulating 100 events with slightly different initial launch points in longitude and latitude ( $\phi, \lambda$ ), we took the more pragmatic approach of flying hypothetical spacecraft through randomly selected parts of the ejecta, within a  $\pm 15^\circ$  cone of the CME center. Although strictly not the same, it effectively allows us to generate multiple realizations for uncertainties in the relative position of the ICME to the Earth. That is, rather than moving the ICME around, we are moving the Earth's position around to generate appropriate realizations.

### 3. Results

We begin by assessing the impact of the background solar wind on ToA uncertainty. For each of the 12 realizations summarized in Figures 1 and 2, we launched an ICME with a speed of  $1,200 \text{ km s}^{-1}$  and a density twice that of the base value. Figure 4 shows the resulting profiles measured at a hypothetical spacecraft located at  $r = 1 \text{ AU}$ ,  $\lambda = 0^\circ$ ,  $\phi = 180^\circ$ , that is, at the center of origin of the ICME. Several points are worth making. First, ADAPT realizations have an important impact on the evolution of the ICME. Speed measurements differ significantly from a peak as low as  $863 \text{ km s}^{-1}$  to as high as  $1,026 \text{ km s}^{-1}$ . This also affects the ToA of the leading edge of the CME disturbance, with the shock arriving over a window of more than 12 h. Similar variations are seen in the other plasma and magnetic field parameters. The importance of this result cannot be overstated. Given that each of these realizations is equally valid, we cannot distinguish between the quality of the forecasts from each one. Thus, we infer that there is an intrinsic limitation of  $\pm 7 \text{ h}$  (the time separating the arrival of the first and last realization at a point one-third of the way up the shock front) based only on our uncertainty in the magnetograms. Moreover, this assumes that the magnetograms represent some kind of “ground truth”. In reality, we know that there are substantially larger differences between synoptic maps generated from different solar observatories (Riley et al., 2014). Thus, the true uncertainties from the choice of magnetograms are likely larger.

We can also analyze the arrival time of the ejecta more precisely by adding tracer particles into the simulation. That is, massless particles that are advected out with the solar wind. By placing them at the leading edge of the CME pulse, we can accurately track their arrival at 1 AU. Figure 5 summarizes the properties of the solar wind at 1 AU, again in the equatorial plane. These are traces of the solar wind that started approximately two days preceding the arrival of CME at Earth. Focusing first on the radial velocity, the ambient solar wind derived from the 12 ADAPT realizations can differ by approximately  $100 \text{ km s}^{-1}$  at both high and low speeds. There are also substantial relative differences in both tangential components of the field. Although it is tempting to conclude that, given the large radial velocity of the CME, these velocities probably do not contribute significantly to differences in arrival time, in fact they do. The dashed lines indicate the ToA for each of the CMEs within each realization, leading to  $\sim \pm 2 \text{ h}$  uncertainty in ToA. Note, however, that the CME arrival times associated with the highest solar wind speed just ahead of them are not always those that arrive first. This is probably related to the fact that when tracking these tracer particles, they are not traveling out radially, but also responding to shearing flows that move them in the transverse direction. Finally, it is worth noting that the uncertainty in ToA computed for the tracer particles ( $\pm 2 \text{ h}$ ) is notably smaller than those estimated from the time of arrival of the CME shock ( $\pm 7 \text{ h}$ ). In the former case, we are

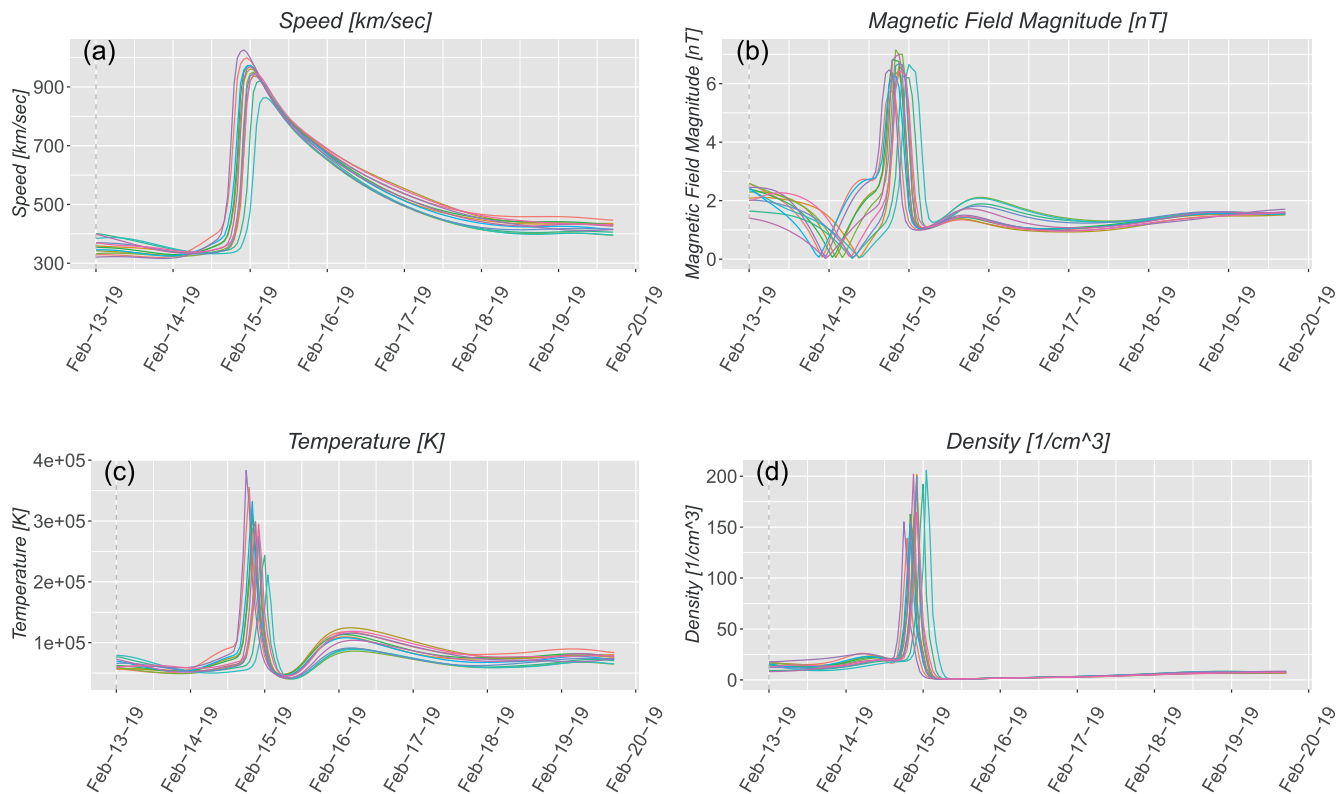


**Figure 4.** Solar wind profiles for a hypothetical coronal mass ejection (CME) launched into the solar wind conditions summarized in Figure 2. The CME had an initial speed of  $1,200 \text{ km s}^{-1}$  and a density twice that of the base value. The dashed line marks the time that the CME was launched from the inner boundary. The panels show: (a) speed, (b) magnetic field magnitude, (c) temperature, and (d) number density.

estimating ToA based on the time history of the particle as it advects through the solar wind, while in the latter, we are identifying the ToA from the passage of a shock (or steepened wave) across the observer's position. Given the non-radial flow, this plasma may be laterally separated significantly from the parcel of plasma that launched at the CME's leading-edge center.

A final point worth making about the profiles in Figure 5 is that, despite the large variations upstream of the ICME from different realizations, none of the plasma shown from February 13 through to early February 15 has any impact upon the ToA of the ICME disturbance nor the deformation of its large-scale structure. Only the plasma directly ahead of the CME can interact with the CME pulse, and, by definition, this is limited to the region downstream of the fast-mode forward shock. Thus, while it is crucial to estimate the properties of the ambient solar wind near to, or surrounding the CME structure, the details of the solar wind away from this region matter little from a forecasting perspective. Of course, currently, there is no way to disentangle the two: large-scale models require global, or near global geometries. Moreover, the properties of the ambient solar wind in the ecliptic plane are modulated, to a large degree, by the properties of the polar magnetic field (Riley et al., 2019) making it less likely that simpler 1-D or 2-D ad hoc approaches can accurately forecast the ambient solar wind into which the CME will be embedded and interact with.

Next, we estimate the impact of uncertainties in the ToA of CMEs based on errors in our estimation of the propagation direction of the CME. Even when multiple spacecraft observe the same event, it is unlikely that the true direction is known to within  $5^\circ$ – $15^\circ$ . As noted above, rather than running a suite of events where we launch an otherwise identical CME in slightly different directions, we can mimic the effect by following the loci of tracer particles within the CME that are spread out by a similar transverse amount, as shown in Figure 6. The two distributions (blue and red) encapsulate the worst ( $\pm 15^\circ$ ) and best ( $\pm 5^\circ$ ) forecast predictions, respectively, based on either one set of coronal observations to constrain the CME, or multiple observations from more than one spacecraft. In the worst case, with only observations from, say, Earth, the CME ToA could likely be forecasted between 40 and 59 h. Or, equivalently,  $\pm 9.5 \text{ h}$  (using 5/95% quantiles).



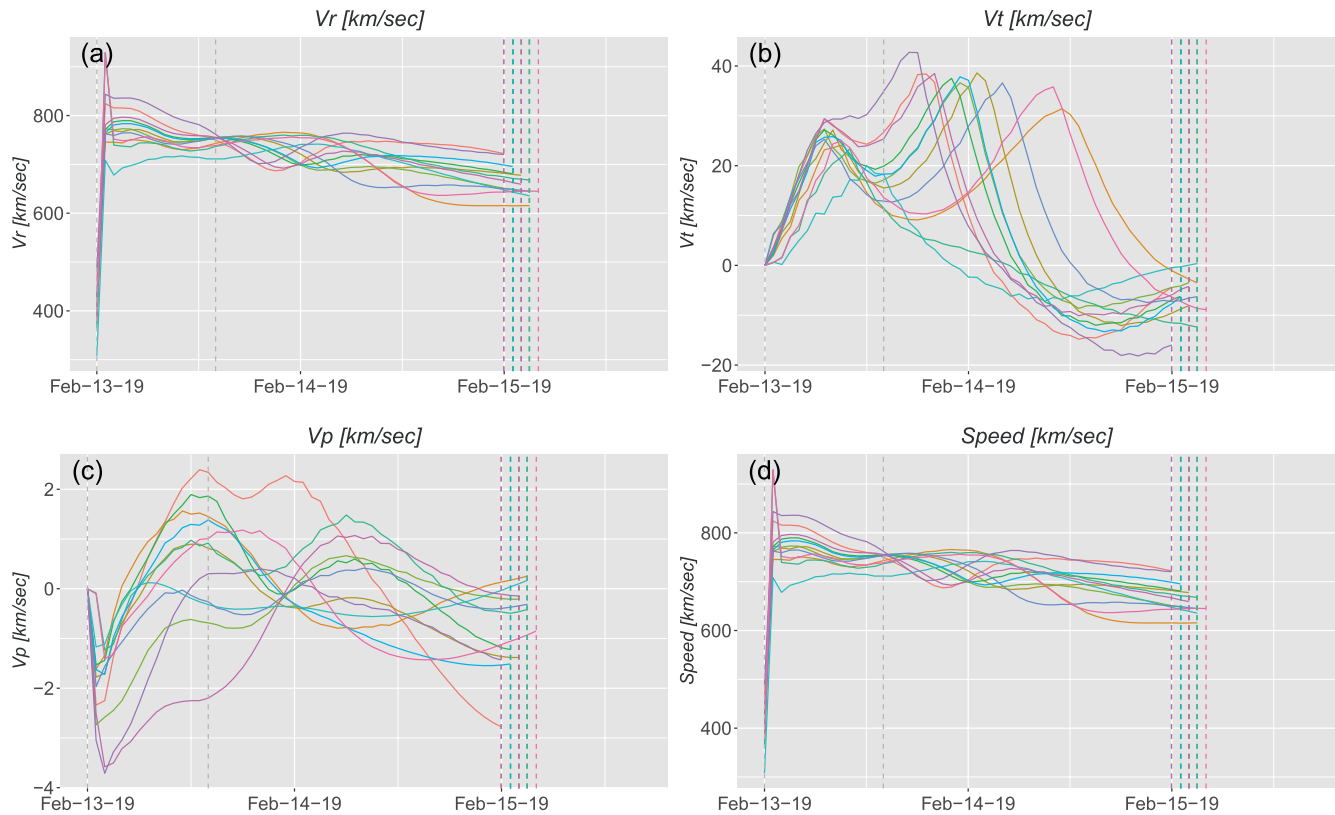


**Figure 5.** (a–c) Upstream velocity components (in spherical coordinates:  $v_r$ ,  $v_\theta$ ,  $v_\phi$ ) and (d) velocity magnitude, for the ambient solar wind realizations shown in Figure 2. The arrival of the interplanetary coronal mass ejection (ICME) propagating through these solutions is indicated by the dashed vertical lines.

This is similar to the uncertainties prevalent in current forecasts of the ToA of ICMEs (Riley et al., 2018). If the uncertainties in the initial direction can be constrained to within  $\pm 5^\circ$ , the associated uncertainties in ToA are substantially reduced, say, between 44 and 58 h, or 5/95% confidence interval (CI):  $\pm 7$  h (For comparison, using mean values and standard deviations would lead to estimates of: 41 and 55 h ( $\pm 7$  h) or 50 and 58 ( $\pm 4$  h), respectively).

We also investigated how uncertainties in the ToA of ICMEs depended on the initial speed of the ICME, which is generally only known to within  $\pm 200$  km s $^{-1}$ , but again dependent on the number and quality of the observations used to derive that estimate. As summarized in Figure 7, we visually infer that for a CME traveling at 1,200, 1,000, and 800 km s $^{-1}$ , the ToA of the first tracer particle was delayed by approximately 4 h for each 200 km s $^{-1}$  drop in initial speed. More quantitatively, we computed the mean, median, range, s.d. and 5/95% CIs for the point where the speed exceeded 500 km s $^{-1}$  (i.e., on the early ascending portion of the shock front). As an example, the median ToA for the 800, 1,000, and 1,200 km s $^{-1}$  ICME was 690, 390, and 210 min, respectively. From this, we can infer that the average uncertainty was 180 (390–210) and 300 (690–390) min between successive ICMEs, or in total, 8 h. Thus, we conclude that (at least for this event) if the speed is known to only within  $\pm 200$  km s $^{-1}$ , the associated uncertainty in ToA is  $\sim \pm 4$  h. Comparing the traces, we can make several remarks. First, prior to the arrival of the shock, all profiles are the same, that is, the only variability is due to the ADAPT realizations. Second, the compression region driven by the speed increase, and visible in the field magnitude, temperature, and density, is centered on the initial speed gradient and, thus, is staggered in time in relation to the phasing of the shock location. Third, the amplitude of the compression is in proportion to the jump in speed, although the fractional change above background values increases from one parameter to the next, with density showing a more than doubling between each of the velocity pulses. Fourth, the rarefaction created on the declining speed profile is proportionately longer for the faster ICME, but the trailing edge of this wave merges into the background flow at roughly the same time for each case. Fifth, the spread in the ToA of the shock front due to (a) the different realizations

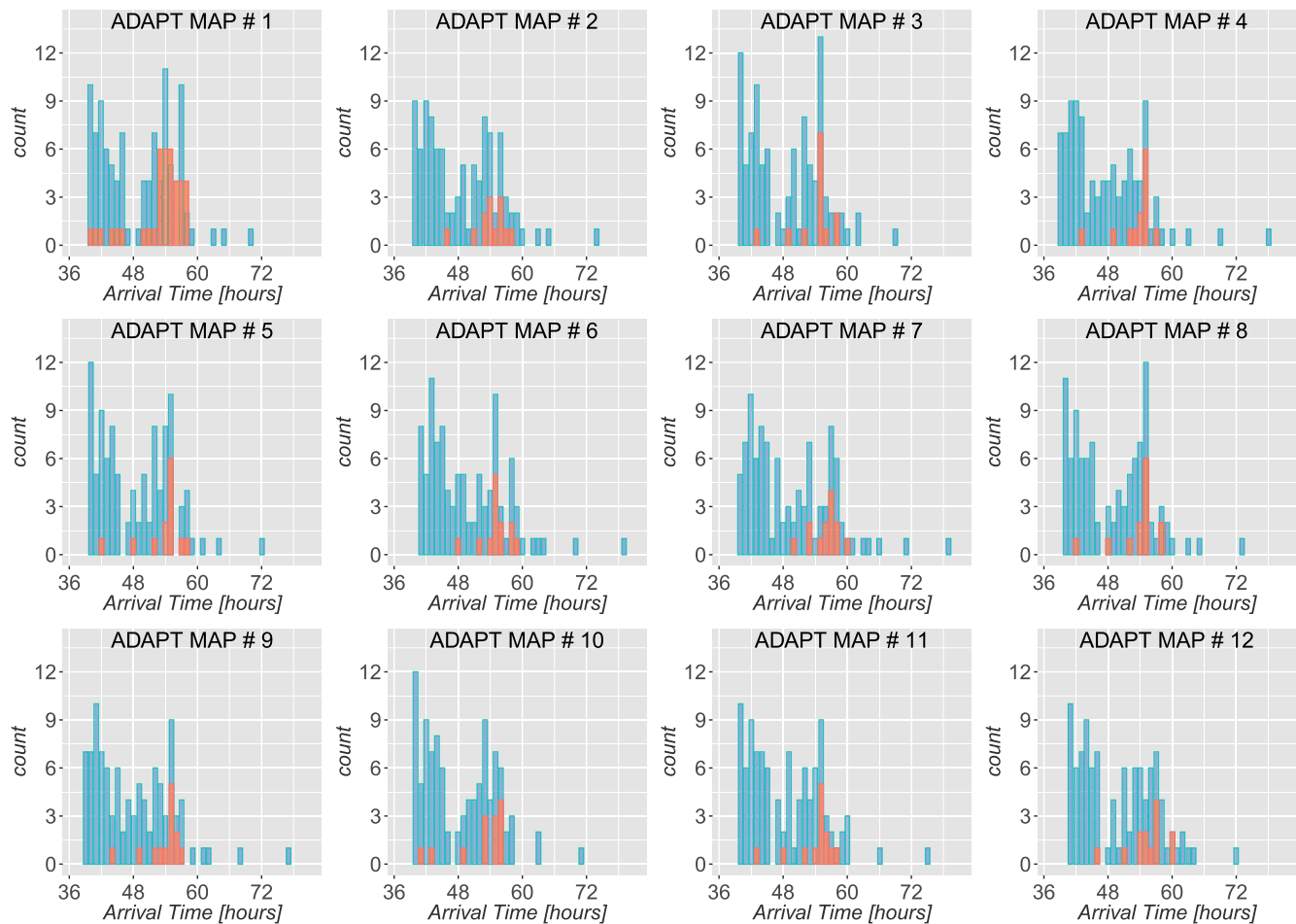


**Figure 6.** Histogram of arrival times for a set of tracer particles embedded at the leading edge of the cone-model CME. The larger (blue) group were all within  $\pm 15^\circ$  of center, while the smaller (red) group were all within  $\pm 5^\circ$  of the center.

(clusters of profiles of the same colors) and (b) the different initial speed jumps (sequential profiles of different colors) are of approximately the same magnitude, suggesting that these sources of uncertainty are roughly comparable.

It is well appreciated that the mass of the CME is one of the most difficult properties to determine with any degree of accuracy (e.g., Vourlidas et al., 2010). To explore what kind of impact this might have, we considered the effects of doubling (or halving) the initial mass within the ejecta. Using the same analysis as described above for uncertainties in CME speed, we found that the difference for mass uncertainties was more modest;  $\sim \pm 2.5$  h separated each ICME profile for a given ambient solar wind realization (Figure 8). Visually, given the fact that the profiles of different colors overlap much more, it is clear that the choice of ADAPT realization has a much larger impact on the ToA than the inferred mass of the CME. However, it is quite conceivable that mass uncertainties are larger than the factor of two assumed here. Unfortunately, even this uncertainty is “uncertain.” In comparison with Figure 7, we also note that modifying the mass of the ICME does not generate the same variations in the structure of the events. That is, ICMEs of the same speed, differing only in mass, produce more dynamically similar events. More massive events arrive sooner, have a modestly higher peak speed, field strength, temperature, and density, but do not have unique features, such as the erosion in peak speed seen in the case of the  $800 \text{ km s}^{-1}$  event in Figure 7.

Finally, the analysis thus far has assumed that we can approximate the uncertainty in the direction of propagation of the ICME by sampling different trajectories through a single simulation. However, this does not account for the fact that different directions of propagation, and particularly changes in latitude, will cause the ICME to interact with different ambient solar wind structure, such as the fast wind that

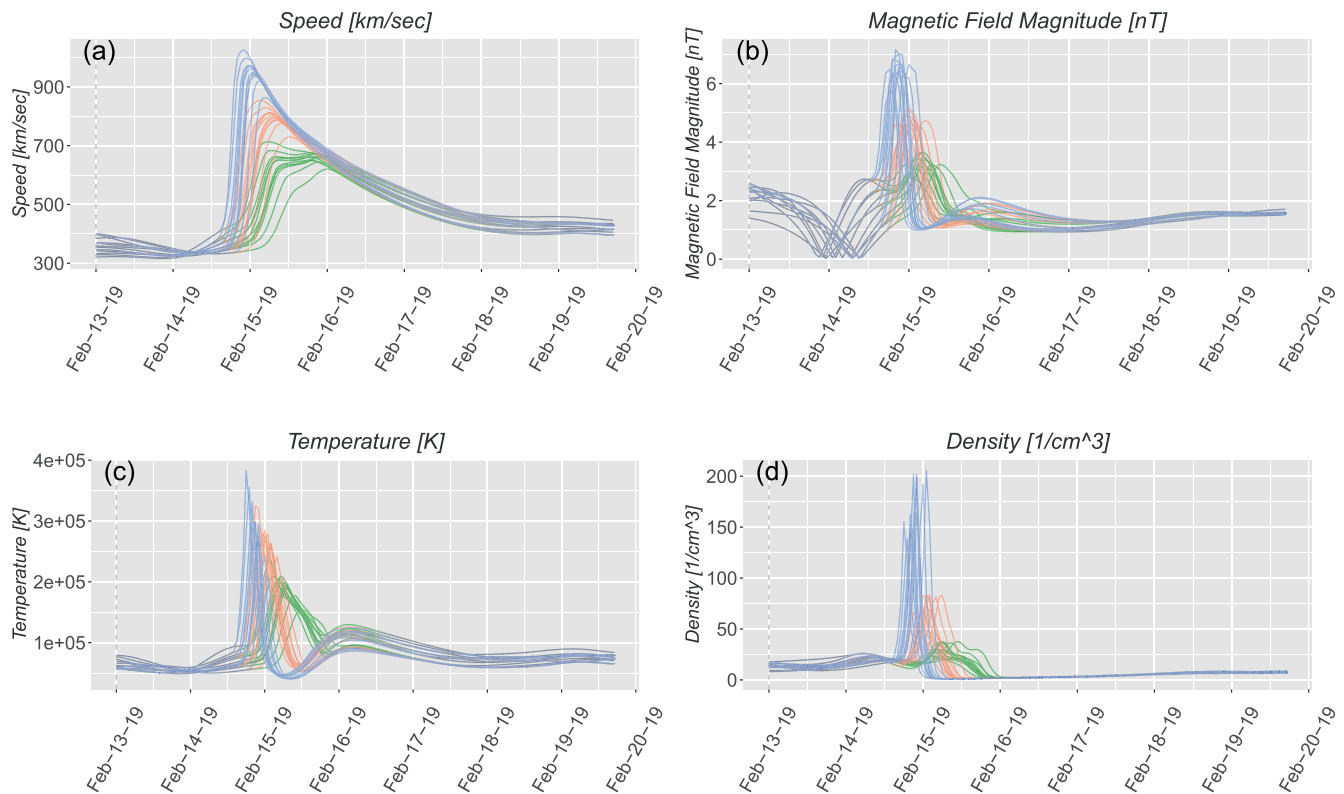


**Figure 7.** Comparison of arrival times for ICMEs with speeds 800 (green), 1,000 (red), and 1,200 (blue)  $\text{km s}^{-1}$ : (a) Speed; (b) magnetic field magnitude; (c) temperature; and (d) density.

entrains the band of slow solar wind about the equator. To explore this, we repeated one of the calculations ( $v_{\text{CME}} = 1,000 \text{ km s}^{-1}$  and  $n_{\text{CME}} = 1,000 \text{ cm}^{-3}$ ), but set the propagation latitude to be 5, 10, and  $15^\circ$  above the heliographic equator. The distribution in arrival times changed in a predictable way. While the fastest ToAs remained the same, other trajectories were dispersed more in time. Even at  $10^\circ$ , the trajectories within  $\pm 5^\circ$  (the red bars in Figure 6) still fell within 48–60 h (although moving progressively further out). However, for the  $15^\circ$  displacement, the  $\pm 5^\circ$  trajectories jumped to the range of 72–84 h, corresponding to the fact that the Earth was now only sampling the outermost flanks and sheath of the ICME.

#### 4. Conclusions and Discussion

In this study, we have investigated the main sources of uncertainties in predicting a CME's ToA at Earth: (a) the initial properties of the ejecta, including its speed, mass, and direction of propagation and (b) the properties of the ambient solar wind into which it propagates. To estimate the relative contribution to ToA uncertainties, we constructed a set of numerical experiments of cone-model CMEs where we varied the initial speed, mass, and direction of the ejecta at the inner heliospheric boundary. Additionally, we built an ensemble of 12 ambient solar wind solutions using realizations from the Air Force's ADAPT model. We found that each point of uncertainty contributed between  $\pm 2.5$  to  $\pm 7$  h of uncertainty to the estimate of the CME's ToA. Importantly, different realizations of the input magnetic synoptic maps resulted in uncertainties of a similar magnitude, suggesting that estimates of ToA will continue to be plagued with intrinsic uncertainties of  $\sim \pm 10$  h until tighter constraints can be found for these boundary conditions, which will likely require more comprehensive observations of the Sun. Finally, our results suggest that there are clear benefits to focused investigations aimed at reducing the uncertainties in CME speed, mass, direction, and input boundary magnetic fields.

Our results explain – to a large degree – the uncertainties found in the forecasts made for the CCMC's “CME Arrival Time Scoreboard” (Riley et al., 2018). A combination of uncertainties in CME speed, direction, and

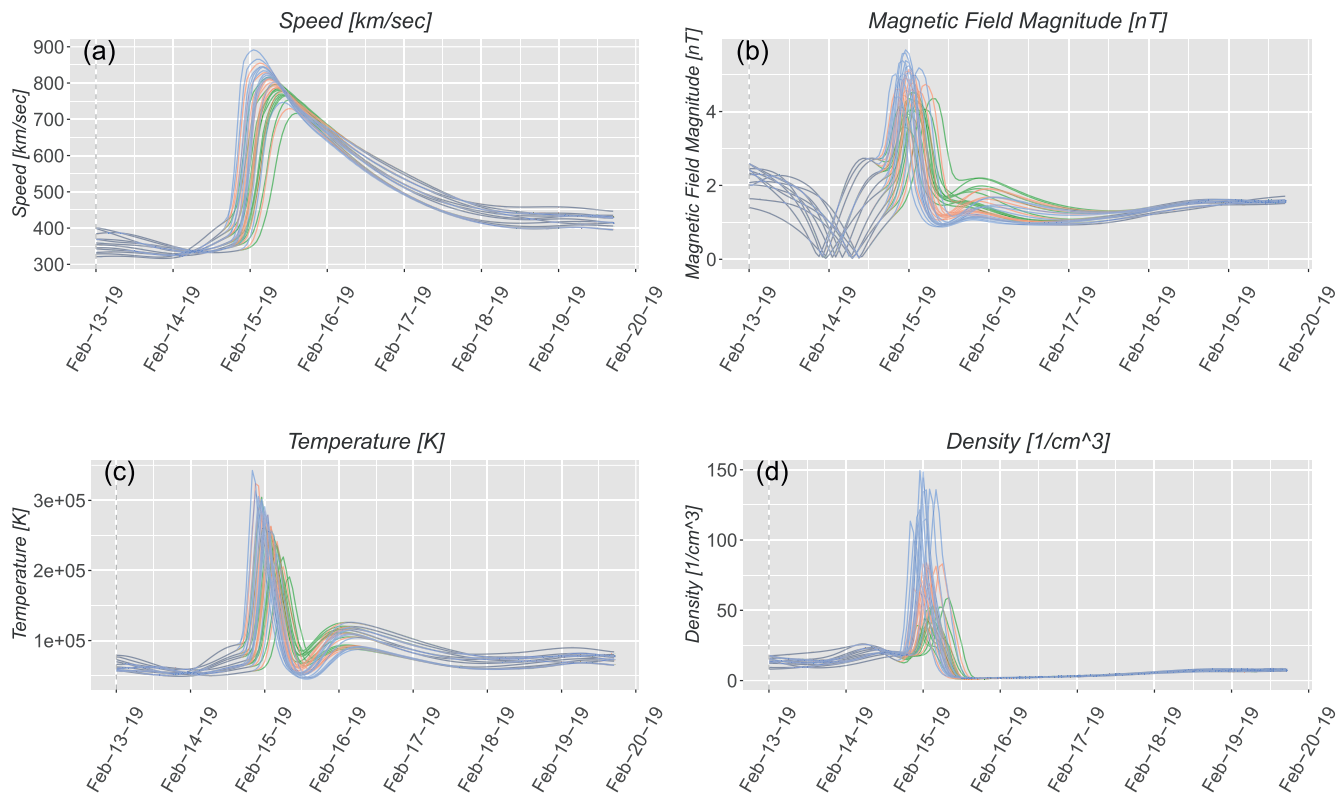


**Figure 8.** Comparison of arrival times for ICMEs density enhancements of  $\times 1$  (green),  $\times 2$  (red), and  $\times 4$  (blue) above background for a  $1,000 \text{ km s}^{-1}$  CME: (a) Speed; (b) magnetic field magnitude; (c) temperature; and (d) density.

mass, as well as uncertainties in the structure of the background solar wind into which the CME is propagating all appear to contribute to varying degrees. It is not surprising, therefore, that none of the models can make estimates where the MAE is smaller than about 12 h. It is worth noting, however, that different models tend to focus on different aspects of the forecasting pipeline. Thus, it may be possible to combine the best practices from different techniques and improve skill scores, at least modestly.

Uncertainties in the properties of the ambient solar wind were shown to have a significant effect in the arrival time of the CME at Earth, in spite of the fact that our analysis was based on only modest differences between each of the 12 realizations calculated for one ADAPT map. As we have demonstrated previously (Riley et al., 2012, 2014), forecasts using magnetogram data from different solar observatories will further increase the differences in the properties of the ambient solar wind, and hence, lead to even larger disparities in the arrival time of the ICME at Earth. These uncertainties, can only be fully addressed by new, comprehensive observations of the Sun that, ideally, would cover  $4\pi$  steradians of the solar surface. In practice, such a mission would require at least two polar-orbiting spacecraft, together with at least three near-ecliptic spacecraft (Riley et al., 2006). In lieu of that, we suggest that modest gains may be obtained from improvements to the data assimilation procedure in the ADAPT map pipeline. A crucial aspect of this would be the extrapolation and “filling in” of missing polar observations, which are key for improving forecasts, even in the ecliptic plane (Riley et al., 2019).

Uncertainties in CME speed, direction, and mass also resulted in significant uncertainties in arrival time. Ultimately, we believe that first-principles models, which include the eruption of the CME and its propagation through the low corona, will produce the most accurate forecasts; however, in analogy with meteorological advances in the 1980s and 1990s, our understanding of the system has not matured to the point that these models can outperform empirical models. Thus, near-term advances will likely come from constraining the properties of the ejecta in the high corona. Analysis of multi-spacecraft white-light observations suggests that this approach can produce more accurate estimates of the initial properties of the CME than



single-spacecraft observations, although this has not yet been demonstrated against global MHD simulations, for which there is an albeit idealized “ground truth.”

Our results are broadly consistent with those of Pizzo et al. (2015), who found that different solutions produced deterministic (non-chaotic) estimates for ToA. Additionally, while we cannot quantitatively compare the dispersion in ToAs directly, the qualitative spread in their parameters (speed, density, and temperature) is consistent with ours (compare their Figures 10, 11, 14, and 16 with our Figures 4–8). Our study also provides an independent assessment that the results of Pizzo et al. (2015) are insensitive to any specific aspects of the forecasting process, including: (a) the particular numerical model being used, (b) the resolution of the simulations, (c) the empirical prescription of the ambient solar wind, (d) the choice of time period under study, and (e) the specification and values of the CME pulses. However, our results extend the Pizzo et al. (2015) study in several important ways. First, we drove the CMEs through realistic ambient backgrounds, modeled using realizations of the observed photospheric magnetic field. Second, we considered uncertainties in the CME pulse profiles that were based on the likely observation uncertainties associated with estimating these parameters (speed, location, and mass) from white-light measurements. And third, we quantified the uncertainties associated with each component in the modeling chain from the Sun to the Earth.

This study is not, however, without limitations or caveats. First, we relied on a global heliospheric MHD algorithm to compute the evolution of the ICME from near the Sun to 1 AU. While the accuracy of such codes has been tested and validated over the years, it is worth noting that these algorithms tend to be numerically diffusive and, as such, tend to dissipate small-scale fluctuations. This likely leads to structures that are more laminar than would be observed. In terms of the results presented here, this would reduce the differences in ToA. Thus, the model results probably underestimate the spread in ToA. Second, and as already noted, our choice of 12 ADAPT realizations also provides a lower limit on the uncertainty in the magnetograms used to drive the ambient solar wind. Both differences in the actual numerical values of the flux as well as how regions that are not well observed (limbs, far-side, and poles) are assembled would produce even greater variability in the maps driving the ambient solutions. Third, our prescription of the CME was limited to a simple hydrodynamic pulse. While this represents the current state-of-the-art, observed CMEs clearly have a strong and significant magnetic structure embedded within them. Thus, once models are capable of reliably incorporating flux rope structures, this will result in an additional degree of uncertainty, dependent on how the properties of the flux rope can be constrained. Fourth, CMEs are often associated with precursor events (e.g., Gopalswamy et al., 2001). This is particularly true for fast, and hence more geo-effective events. These can either provide a means for sweeping out ambient solar wind structure ahead of the CME under consideration, or act as an obstacle that the following CME interacts with. In either case, this added complexity will also act to disperse the predicted ToAs, that is, it will increase the uncertainty in the forecasts. Fifth, the ambient solar wind conditions we chose were representative of late declining phase conditions. It is not clear how our results would change near the maximum of the solar cycle. On one hand, the more organized pattern of slow flow around the heliomagnetic equator and steady fast wind beyond that would be replaced with more variable wind at all latitudes, suggesting more variability. However, on the other hand, with more localized sources of faster wind, peaks in solar wind speed are more readily eroded, and slower solar wind is more easily accelerated, perhaps resulting in a net narrowing in the spread of arrival times. This remains an interesting question for future studies.

In this study, by design, we did not study an observed event. We were not attempting to uncover the “correct” answer. Instead, our goal was to quantify the sources of uncertainty in the ToA of CMEs. Forecasting observed events is, ultimately, a more important objective. However, in the case of predicting observed events, care must be taken to avoid biasing the results by adjusting input parameters to more closely match the observations. True forecasts, such as those submitted to the CCMC’s “CME Arrival Time Scoreboard” avoid this problem by requiring submissions prior to the arrival of the CME at 1 AU. On the other hand, hindcasts, or “retrospective forecasts” can potentially result in overly-optimistic results, since the analyst may (inadvertently) adjust input parameters to improve the forecast, in which case, the forecast is more of a curve fitting exercise than a demonstration of a promising technique. Nevertheless, when applied over a sufficiently large number of events, this could provide important information for constraining the free parameters of the model. The final test, however, remains to predict future events, such as through the CCMC

portal, and this should be an objective for any ICME forecasting tool. In the interim, rigorous hindcast exercises could be conducted using the events cataloged at the CCMC portal, together with code made available to compare the new model's results with those that originally made the forecasts (Riley et al., 2018).

The study described here focused on the sources of uncertainty in predicting the ToA of ICMEs; however, the model results contain a wealth of other information that could be assessed in more depth, such as the properties of the ejecta and the shocks driven by them. While we plan to continue our investigation, we have also published all model results and analysis codes allowing other researchers to both verify and extend our results. Additionally, we are completing the development of a new open-source global ICME code that will allow us to study possible errors introduced by the specific choice of the numerical algorithms used to compute the solutions.

In closing, based on the results presented here, we suggest that there are fundamental limitations to the accuracy that current CME forecasting tools can achieve. Modest advances can be made by more thorough analyses, including comprehensive efforts to “hindcast” many ICME events and use robust statistical approaches to better constrain free parameters. However, ultimately, the greatest improvements will only come from a substantial investment in the form of multi-viewpoint observations of the photospheric magnetic field and white-light images of the corona.

## Data Availability Statement

All model results analyzed in this study are available from the following repository: Ben-Nun and Riley (2021).

## Acknowledgments

The authors gratefully acknowledge support from NASA (80NSSC18K0100, NNX16AG86G, 80NSSC18K1129, 80NSSC18K0101, 80NSSC20K1285, 80NSSC18K1201, and NNN06AA01C), NOAA (NA18NWS4680081), and the U.S. Air Force (FA9550-15-C-0001).

## References

- Amerstorfer, T., Hinterreiter, J., Reiss, M. A., Möstl, C., Davies, J. A., Bailey, R. L., et al. (2021). Evaluation of CME arrival prediction using ensemble modeling based on heliospheric imaging observations. *Space Weather*, 19(1), e2020SW002. <https://doi.org/10.1029/2020sw002553>
- Arge, C. N., Henney, C. J., Koller, J., Compeau, C. R., Young, S., MacKenzie, D., et al. (2010). Air force data assimilative photospheric flux transport (ADAPT) model. In M. Maksimovic, K. Issautier, N. Meyer-Vernet, M. Moncuquet, & F. Pantellini (Eds.), *Twelfth International Solar Wind Conference. AIP Conference Proceedings* (Vol. 1216, pp. 343–346). <https://doi.org/10.1063/1.3395870>
- Arge, C. N., Odstrcil, D., Pizzo, V. J., & Mayer, L. R. (2003). Improved method for specifying solar wind speed near the Sun. In M. Velli, R. Bruno, F. Malara, & B. Bucci (Eds.), *Solar Wind Ten, American Institute of Physics Conference Series* (Vol. 679, pp. 190–193). <https://doi.org/10.1063/1.1618574>
- Ben-Nun, M., & Riley, P. (2021). *On the sources and sizes of uncertainty in predicting the arrival time of interplanetary coronal mass ejections using global MHD models*. <https://osf.io/c3927/>
- Dumbović, M., Čalogović, J., Vršnak, B., Temmer, M., Mays, M. L., Veronig, A., & Piantischitsch, I. (2018). The drag-based ensemble model (DBEM) for coronal mass ejection propagation. *The Astrophysical Journal*, 854(2), 180.
- Forbes, T. G., & Lin, J. (2000). What can we learn about reconnection from coronal mass ejections. *Journal of Atmospheric and Solar-Terrestrial Physics*, 62, 1499–1507. [https://doi.org/10.1016/S1364-6826\(00\)00083-3](https://doi.org/10.1016/S1364-6826(00)00083-3)
- Gopalswamy, N., Yashiro, S., Kaiser, M. L., Howard, R. A., & Boueret, J. L. (2001). Radio signatures of coronal mass ejection interaction: Coronal mass ejection cannibalism? *The Astrophysical Journal*, 548(1), L91–L94. <https://doi.org/10.1086/318939>
- Gosling, J. T., Bame, S. J., McComas, D. J., & Phillips, J. L. (1990). Coronal mass ejections and large geomagnetic storms. *Geophysical Research Letters*, 17, 901–904. <https://doi.org/10.1029/gl017i007p00901>
- Iwai, K., Shiota, D., Tokumaru, M., Fujiki, K., Den, M., & Kubo, Y. (2019). Development of a coronal mass ejection arrival time forecasting system using interplanetary scintillation observations. *Earth Planets and Space*, 71(1), 39. <https://doi.org/10.1186/s40623-019-1019-5>
- Jackson, B., Hick, P., Buffington, A., Yu, H.-S., Bisi, M., Tokumaru, M., & Zhao, X. (2015). A determination of the north–south heliospheric magnetic field component from inner corona closed-loop propagation. *The Astrophysical Journal Letters*, 803(1), L1. <https://doi.org/10.1088/2041-8205/803/1/L1>
- Kay, C., Mays, M., & Verbeke, C. (2020). Identifying critical input parameters for improving drag-based CME arrival time predictions. *Space Weather*, 18(1), e2019SW002. <https://doi.org/10.1029/2019sw002382>
- Mays, M., Taktakishvili, A., Pulkkinen, A., MacNeice, P., Rastätter, L., Odstrcil, D., et al. (2015). Ensemble modeling of CMEs using the WSA-ENLIL+ cone model. *Solar Physics*, 290(6), 1775–1814. <https://doi.org/10.1007/s11207-015-0692-1>
- Odstrcil, D., Riley, P., Linker, J. A., Lionello, R., Mikic, Z., & Pizzo, V. J. (2003). 3-D simulations of ICMEs by coupled coronal and heliospheric models. In *ESA SP-535: Solar variability as an input to the Earth's environment* (p. 541–546).
- Odstrcil, D., Riley, P., & Zhao, X. P. (2004). Numerical simulation of the 12 May 1997 interplanetary CME event. *Journal of Geophysical Research*, 109, A02116. <https://doi.org/10.1029/2003JA010135>
- Pizzo, V., Koning, C., Cash, M., Millward, G., Biesecker, D., Puga, L., et al. (2015). Theoretical basis for operational ensemble forecasting of coronal mass ejections. *Space Weather*, 13(10), 676–697. <https://doi.org/10.1002/2015sw001221>
- Pizzo, V., Millward, G., Parsons, A., Biesecker, D., Hill, S., & Odstrcil, D. (2011). Wang-Sheeley-Arge-Enlil cone model transitions to operations. *Space Weather*, 9, 03004. <https://doi.org/10.1029/2011SW000663>
- Pomell, J., & Poedts, S. (2018). EUHFORIA: European heliospheric forecasting information asset. *Journal of Space Weather and Space Climate*, 8, A35. <https://doi.org/10.1051/swsc/2018020>

- Riley, P., Ben-Nun, M., Linker, J. A., Mikic, Z., Svalgaard, L., Harvey, J., et al. (2014). A multi-observatory inter-comparison of line-of-sight synoptic solar magnetograms. *Solar Physics*, 289, 769–792. <https://doi.org/10.1007/s11207-013-0353-1>
- Riley, P., & Gosling, J. T. (1998). Do coronal mass ejections implode in the solar wind? *Geophysical Research Letters*, 25, 1529–1532. <https://doi.org/10.1029/98gl01057>
- Riley, P., Linker, J. A., & Arge, C. N. (2015). On the role played by magnetic expansion factor in the prediction of solar wind speed. *Space Weather*, 13(3), 154–169. <https://doi.org/10.1002/2014sw001144>
- Riley, P., Linker, J. A., Lionello, R., & Mikic, Z. (2012). Corotating interaction regions during the recent solar minimum: The power and limitations of global MHD modeling. *Journal of Atmospheric and Solar-Terrestrial Physics*, 83, 1–10. <https://doi.org/10.1016/j.jastp.2011.12.013>
- Riley, P., Linker, J. A., & Mikić, Z. (2001). An empirically-driven global MHD model of the corona and inner heliosphere. *Journal of Geophysical Research*, 106(15), 889–15901. <https://doi.org/10.1029/2000JA000121>
- Riley, P., Linker, J. A., Mikic, Z., Caplan, R. M., Downs, C., & Thumm, J.-L. (2019). Can an unobserved concentration of magnetic flux above the poles of the Sun resolve the open flux problem? *The Astrophysical Journal*, 884(1), 18. <https://doi.org/10.3847/1538-4357/ab3a98>
- Riley, P., Linker, J. A., Mikic, Z., & Lionello, R. (2006). Maximizing the scientific return of the Sentinels mission using global MHD models. In AGU Fall Meeting Abstracts (p. C4).
- Riley, P., Linker, J. A., Mikić, Z., Odstrcil, D., Zurbuchen, T. H., Lario, D., & Lepping, R. P. (2003). Using an MHD simulation to interpret the global context of a coronal mass ejection observed by two spacecraft. *Journal of Geophysical Research*, 108, 1272. <https://doi.org/10.1029/2002ja009760>
- Riley, P., Mays, M. L., Andries, J., Amerstorfer, T., Biesecker, D., Delouille, V., et al. (2018). Forecasting the arrival time of coronal mass ejections: Analysis of the CCMC CME scoreboard. *Space Weather*, 16(9), 1245–1260. <https://doi.org/10.1029/2018sw001962>
- Shiota, D., & Kataoka, R. (2016). Magnetohydrodynamic simulation of interplanetary propagation of multiple coronal mass ejections with internal magnetic flux rope (SUSANOO-CME). *Space Weather*, 14(2), 56–75. <https://doi.org/10.1002/2015sw001308>
- Török, T., Downs, C., Linker, J. A., Lionello, R., Titov, V. S., Mikić, Z., et al. (2018). Sun-to-Earth MHD simulation of the 2000 July 14 “Bastille Day” eruption. *The Astrophysical Journal*, 856(1), 75. <https://doi.org/10.3847/1538-4357/aab36d>
- Verbeke, C., Mays, M., Temmer, M., Bingham, S., Steenburgh, R., Dumbović, M., et al. (2019). Benchmarking CME arrival time and impact: Progress on metadata, metrics, and events. *Space Weather*, 17(1), 6–26. <https://doi.org/10.1029/2018sw002046>
- Vourlidas, A., Howard, R. A., Esfandiari, E., Patsourakos, S., Yashiro, S., & Michalek, G. (2010). Comprehensive analysis of coronal mass ejection mass and energy properties over a full solar cycle. *The Astrophysical Journal*, 722(2), 1522–1538. <https://doi.org/10.1088/0004-637x/722/2/1522>